JOURNAL OF CATALYSIS 119, 451–466 (1989)

The Genesis of Carbon-Supported Fe–Mn and K–Fe–Mn Catalysts from Stoichiometric Metal Carbonyl Clusters

III. Characterization by Chemisorption, Calorimetry, and Kinetic Analysis

JEREMY J. VENTER, ANDREW A. CHEN, JONATHAN PHILLIPS, AND M. ALBERT VANNICE*

Department of Chemical Engineering, The Pennsylvania State University, University Park, Pennsylvania 16802

Received January 27, 1989; revised June 7, 1989

Carbon-supported Fe, Fe–Mn, and K–Fe–Mn catalysts derived from stoichiometric mixed-metal carbonyl clusters were pretreated at either 473 or 673 K in H_2 after which their chemisorption behavior and catalytic properties for CO hydrogenation were determined. The iron remained well-dispersed at all times except after high temperature reduction when potassium was present. The single promotion by either Mn or K increased the olefin/paraffin ratio, and the doubly promoted catalyst gave very high selectivity to light olefins. Integral CO heats of adsorption at 300 K were measured, and they increased from 15 kcal/mole on the Fe/C catalysts to nearly 17 kcal/mole on each singly promoted sample to 21 kcal/mole on the doubly promoted catalyst. A model for the decomposition of these carbonyl clusters is proposed based on these results combined with previous studies utilizing Mössbauer effect spectroscopy, transmission election microscopy/energy dispersive spectroscopy, and diffuse reflectance Fourier transform infrared spectroscopy. The state of the MnO_x and K phases on the iron surface, as well as Fe crystallite size, appears to play a dominant role in determining catalytic behavior.

INTRODUCTION

Although CO hydrogenation has received much attention in the past, the ability to selectively produce chemical intermediates such as lower molecular weight olefins still remains a challenging task. Fe catalysts promoted by alkali metals provided some increase in olefin yields (*1*, *2*); however, the discovery that addition of Mn to Fe Fischer–Tropsch catalysts can markedly enhance olefin yields is relatively recent (*3–5*). Many subsequent studies have been conducted on both unsupported and supported promoted Fe–Mn catalysts, and these studies have been cited and discussed in our initial publications on the behavior of carbon-supported Fe–Mn catalysts (*6*, *7*) as well as in the first paper in this series (*8*). The reasons for this enhancement in olefin formation are still not clear, although postulates have been made invoking structurally promoted Fe particles, mixed oxide phases, or a combination of electronic and structural promotion (*6*).

Our particular interest stems from the fact that well-dispersed, carbon-supported Fe–Mn catalysts prepared from metal carbonyl clusters not only give very high selectivities to light olefins but also produce higher activities per gram Fe than those reported for bulk Fe–Mn catalysts (*6*, *7*). To clarify the chemistry associated with the genesis of these Fe–Mn and K–Fe–Mn catalysts as they are formed by the decomposition of stoichiometric mixed-metal clusters and to identify the chemical states present before and after catalysis of the CO hydrogenation reaction, diffuse reflectance infrared Fourier transform spectroscopy (DRIFTS), Mössbauer effect spectroscopy (MES), and transmission electron microscopy/energy dispersive spectroscopy (TEM/EDS) were used in comple-

* To whom correspondence should be addressed.

0021-9517/89 $3.00

mentary studies to monitor the species formed from these Fe–Mn carbonyl clusters on a clean carbon support (*8, 9*). The decarbonylation of the mixed-metal carbonyl cluster led to the formation of intermediate $Mn_2(CO)_{10}$ and $[HFe_4(CO)_{13}]^-$ species which appeared to remain in close proximity to each other throughout the decomposition process and to ultimately produce small reduced Fe crystallites. In the present study, the state of the catalyst after different pretreatments and the use of various mixed-metal carbon cluster precursors was probed by H_2 and CO adsorption, CO heat of adsorption measurements, and the CO hydrogenation reaction. This paper proposes the decomposition steps that occur during each pretreatment and associates the chemical state of the Fe–Mn catalysts with the observed adsorption and catalytic properties. Also, this study again illustrates the uniqueness of carbon supports compared to the use of refractory metal oxides which can oxidize these clusters (*10*).

EXPERIMENTAL

The catalysts and their preparation without air exposure from $Fe_3(CO)_{12}$, $Mn_2(CO)_{10}$, $NEt_4[Fe_2Mn(CO)_{12}]$, $K[Fe_2Mn(CO)_{12}]$, and $K[HFe_3(CO)_{11}]$ using Schlenk line techniques are described in detail elsewhere (*6, 8, 11*); they will be abbreviated as Fe_3/C, Mn_2/C, Fe_2Mn/C, KFe_2Mn/C, and KFe_3/C, respectively. The subscripts, however, do not imply the existence of metal particles with that stoichiometry after decomposition. The equipment used for the chemisorption, kinetic, and calorimetric measurements has also been described previously (*8, 9, 12*). Chemisorption of CO and H_2 on the fresh catalyst was measured after a low temperature reduction (LTR) at 473 K as well as a high temperature reduction (HTR) at 673 K whereas the used samples (after the kinetic runs) were characterized following a HTR step. Details are given elsewhere (*13, 14*). CO chemisorption was determined using a dual isotherm method (*15*), while H_2 desorption after cooling in H_2 from the reduction temperature was used to determine H_2 uptakes (*16*). The kinetic measurements were obtained at 1 atm under differential conditions using a glass, plug-flow microreactor system (*6*). The activities for CO hydrogenation were obtained after either a LTR or a HTR pretreatment using a bracketing technique to avoid deactivation (*17*), and partial pressure analyses were performed after HTR using He as the diluent in the feed stream. The pressure dependencies were obtained using a power rate law over fairly narrow ranges of 0.1 to 0.4 atm CO at a constant H_2 pressure of 0.6 atm and of 0.2 to 0.8 atm H_2 at a constant CO pressure of 0.2 atm. The isothermal energy changes during CO adsorption were measured in a modified Perkin–Elmer DSC-2C differential scanning calorimeter (*18*). The only additional modification required was the installation of a small N_2-purged glovebox which allowed the transfer of catalyst into the DSC without air exposure. Calorimetric and adsorption measurements were conducted in parallel on samples derived from a single batch of catalyst. The catalysts in both systems were subjected to identical treatments, which provided reproducible heats of adsorption on two samples of each catalyst (*12*).

RESULTS

The catalysts and their metal loadings were reported earlier (*8*). The total (Fe + Mn) loadings varied between 6.5 and 10.2 wt%, while the Fe content varied between 5.0 and 8.7 wt%, each of which was approximately double that utilized in a previous study of Fe–Mn/C catalysts (*6, 7*).

The chemisorption measurements on the fresh catalysts after either LTR or HTR are listed in Table 1. The adsorption of H_2 or CO on Mn is near zero (*6*), so that the uptakes can be associated only with the iron. This provides a measure of the adsorption sites on Fe and an estimate of Fe dispersion (fraction exposed) if the CO uptake at 195

TABLE 1

Initial Chemisorption Measurements on Fe–Mn/C Catalysts Derived from Metal Carbonyl Clusters

Catalyst precursor	Wt% Fe	H_2 or CO uptake (μmole/g cat)						Adsorption ratios based on total Fe					
		LTR			HTR			LTR[a]			HTR[a]		
		H_2	CO 195 K	CO 300 K	H_2	CO 195 K	CO 300 K	H/Fe	CO/Fe 195 K	CO/Fe 300 K	H/Fe	CO/Fe 195 K	CO/Fe 300 K
$Fe_3(CO)_{12}$–*A*	8.7	57	450	583	84	469	395	0.07	0.29	0.38	0.11	0.30	0.25
$Fe_3(CO)_{12}$–*B*	6.5	57	434	578	79	403	367	0.10	0.38	0.50	0.14	0.35	0.32
$NEt_4[Fe_2Mn(CO)_{12}]$	5.0	72	65	47	79	285	292	0.16	0.07	0.05	0.18	0.32	0.33
$Mn_2(CO)_{10}$	—	—	—	—	—	—	—	—	—	—	—	—	—
$K[HFe_3(CO)_{11}]$	7.2	46	150	109	61	464	176	0.07	0.12	0.09	0.10	0.36	0.14
$K[Fe_2Mn(CO)_{12}]$	5.3	55	102	73	97	372	195	0.12	0.11	0.08	0.20	0.39	0.20

[a] μmoles adsorbed/μmoles $(Fe)_{total}$.
[b] Based on CO (195 K) assuming $CO_{ad}/Fe_s = 0.5$.

K is used, at which temperature no Fe carbonyls form (*8*), and an adsorption ratio of $CO_{ad}/Fe_s = 0.5$ is assumed (*19*). The adsorption measurements indicated that well-dispersed Fe_3/C catalysts were derived from $Fe_3(CO)_{12}$ after either a LTR or a HTR step, consistent with previous work (*6, 20, 21*). After completion of the kinetic studies, the used Mn_2/C catalyst showed no uptake of either H_2 or CO, as expected (*22–27*). After a LTR step, the Fe_2Mn/C catalyst showed only very small uptakes of H_2 or CO at either 195 or 300 K, which gave CO/Fe ratios of 0.05 and 0.07, respectively; however, these uptake ratios increased significantly to over 0.3 following a HTR treatment. The KFe_3/C and KFe_2Mn/C catalysts showed similar behavior, as the CO/Fe ratios at 195 K increased from around 0.1 to near 0.4 following a HTR treatment. Consistent with an earlier study of very small reduced Fe particles by Topsoe *et al.* (*28*), the H/Fe ratios were 2–4 times lower than the CO/Fe ratios. After a HTR pretreatment, the CO uptakes at 300 and 195 K were very similar for the unpromoted catalysts but the CO uptake at 300 K was significantly lower than that at 195 K for the K-promoted catalysts. After the HTR step, apparent Fe dispersions of 0.6 to 0.8 were obtained for the catalysts without K. These catalysts gave no Fe X-ray diffraction pattern and no Fe crystallites were distinguishable by TEM (*9*), thus highly dispersed catalysts were obtained as before (*6*), even though the metal loadings were approaching 10 wt%.

Chemisorption measurements following the kinetic investigations are listed in Table 2. The catalysts showed high uptakes of CO at either 195 or 300 K, but each uptake was lower than that determined on the fresh sample. This is most likely due to sintering under reaction conditions, but a greater inhibition due to promoter rearrangement cannot be completely discounted. Regardless, the reduction in the available Fe surface area was only 10–20%. The H_2 uptake on each sample was again only $\frac{1}{3}$ to $\frac{1}{2}$ of the CO uptakes, as expected for very small Fe crystallites (*28*). For the catalysts without potassium, the CO uptake at 300 K was similar to that at 195 K, whereas it was much lower on the K-promoted catalysts, as found previously (*6, 7*).

The catalytic activities at our standard conditions of 0.1 MPa (1 atm) and 548 K after either a LTR or a HTR treatment are listed in Table 3. Specific activities are normalized to the amount of iron in order to determine the influence of the two additives, Mn and K, which are inactive by themselves. Turnover frequencies (TOFs) are defined as molecules CO reacted per second per Fe_s (surface Fe atom) as calculated based on CO uptakes at 195 K.

TABLE 2

Chemisorption Measurements on Fe–Mn/C Catalysts Derived from Metal Carbonyl Clusters Following Kinetic Measurements

Catalyst	H_2 or CO uptake $\left[\frac{\mu moles}{g\ cat}\right]$			Adsorption ratios based on total Fe[a]				$\frac{Fe_s}{Fe_t}$[c]
	H_2	CO 195 K	CO 300 K	H/Fe	CO/Fe 195 K	CO/Fe 300 K	O (300 K)/CO 195 K	
$Fe_3(CO)_{12}$–*A*	86	371	368	0.11	0.24	0.24	1.0	0.48
$Fe_3(CO)_{12}$–*B*	83	356	312	0.14	0.31	0.27	0.9	0.62
$NEt_4[Fe_2Mn(CO)_{12}]$	77	259	254	0.17	0.29	0.29	1.0	0.58
$Mn_2(CO)_{10}$	27	69	1	0.04[b]	0.05[b]	0.00[b]	0.0	—
$K[HFe_3(CO)_{11}]$	78	386	100	0.12	0.30	0.08	0.3	0.60
$K[Fe_2Mn(CO)_{12}]$	84	314	90	0.12	0.33	0.09	0.3	0.66

[a] μmoles/μmoles $(Fe)_{total}$.
[b] μmoles/μmoles $(Mn)_{total}$.
[c] Based on CO_{ad} at 195 K assuming $CO/Fe_s = 0.5$.

After either pretreatment the two Fe_3/C catalysts had the highest activities, and TOFs for CO conversion to hydrocarbons over the unpromoted catalysts were near 0.002 s^{-1} after a LTR step and they doubled after a HTR step, presumably because of an increase in Fe crystallite size (*13*). The Fe_2Mn/C catalyst had a much lower spe-

TABLE 3

Activity of Fe–Mn/C Catalysts Derived from Metal Carbonyl Clusters

Catalyst	Wt% Fe	Specific activity[a] $\left(\frac{\mu moles\ CO\ reacted}{\mu moles\ Fe \cdot s}\right) * 10^3$			CO TOF[b] ($s^{-1} * 10^3$)	
		CO_2	HC	CH_4	To HC	To CH_4
LTR						
$Fe_3(CO)_{12}$–*A*	8.7	1.45	1.17	0.20	2.0	0.35
$Fe_3(CO)_{12}$–*B*	6.5	1.82	1.30	0.30	1.7	0.40
$NEt_4[Fe_2Mn(CO)_{12}]$	5.0	0.22	0.19	0.033	1.3	0.20
$Mn_2(CO)_{10}$	0	—	—	—	0.0	0.00
$K[HFe_3(CO)_{11}]$	7.2	1.20	0.44	0.078	1.9	0.35
$K[Fe_2Mn(CO)_{12}]$	5.3	0.60	0.14	0.018	0.7	0.10
HTR						
$Fe_3(CO)_{12}$–*A*	8.7	2.43	2.58	0.58	5.4	1.20
$Fe_3(CO)_{12}$–*B*	6.5	2.46	2.06	0.51	3.3	0.82
$NEt_4[Fe_2Mn(CO)_{12}]$	5.0	0.89	0.68	0.15	1.1	0.26
$Mn_2(CO)_{10}$	0	0.00	0.00	0.00	0.0	0.00
$K[HFe_3(CO)_{11}]$	7.2	1.13	0.55	0.10	0.9	0.17
$K[Fe_2Mn(CO)_{12}]$	5.3	1.47	0.83	0.11	1.3	0.17

[a] $T = 548$ K, $P = 1$ atm, $H_2/CO = 3:1$.
[b] Based on CO adsorption at 195 K on fresh samples for runs after LTR pretreatment and on used samples after HTR pretreatment ($CO : Fe_s = 0.5$, assumed).

cific activity (per Fe) after LTR, but the TOF of 0.0013 s^{-1} was only slightly lower than those for the Fe_3/C catalysts. Subjecting this catalyst to HTR significantly enhanced both the specific activity and the CO uptake at 195 K, so that the TOF changed little and remained somewhat lower than those for the Fe_3/C catalysts. Thus the addition of Mn to the cluster decreased activity after either pretreatment. The Mn_2/C catalyst was inactive after either pretreatment.

The influence of K-promotion on the catalytic activity is illustrated by the behavior of the catalyst obtained from $K[HFe_3(CO)_{11}]$, which had a similar TOF after an LTR step but a specific activity (per g Fe) about one-third that of the unpromoted Fe_3/C catalysts. The formation of CO_2 relative to hydrocarbon formation, however, was noticeably increased. Following a HTR step the activity increased slightly but the TOF dropped by one-half. The influence of adding both these elements is illustrated by the KFe_2Mn/C catalyst, which showed the lowest specific activity and TOF after a LTR pretreatment. After HTR, however, this catalyst had a specific activity and TOF similar to those of the Fe_2Mn/C and KFe_3/C catalysts, with all three catalysts being less active than the Fe_3/C catalysts. At these loadings potassium and manganese, either separately or together, reduce both the specific activity and the TOF of these small Fe particles.

In Table 4 the product distributions of these catalysts are given over a narrow range of CO conversion because selectivities, especially the olefin/paraffin ratio (OPR), can be very dependent upon this variable. The Fe_3/C catalysts after either LTR or HTR showed product distributions very similar to those reported previously for Fe_3/C catalysts with lower loadings (*6, 13, 19–21*), and gave C_2–C_4 OPRs between 0.8 and 1.6, which are higher than those obtained over large, unpromoted Fe crystallites but similar to those for very small Fe particles (*13, 19*). The Fe_2Mn/C catalyst after LTR showed a marked enhancement in olefin formation as an OPR of 5.1 was obtained, but this selectivity was irreversibly changed to that of an iron-only catalyst following HTR. Again, this behavior is similar to that observed previously for a catalyst with a lower loading of this cluster (*6,*

TABLE 4

Selectivity of Fe–Mn/C Catalysts Derived from Metal Carbonyl Clusters

Catalyst	Temp. (°C)	CO conversion to HC (%)	Selectivity (mole% hydrocarbons)								OPR $\left[\frac{C_2^= + C_3^=}{C_2 + C_3}\right]$	α
			C_1	$C_2^=$	C_2	$C_3^=$	C_3	$C_4^=$	C_4	C_{5+}		
LTR												
$Fe_3(CO)_{12}$–*A*	202	1.8	43	12	11	12	4	2	9	7	1.6	0.57
$Fe_3(CO)_{12}$–*B*	201	1.6	47	8	13	12	3	1	7	9	1.3	0.55
$NEt_4[Fe_2Mn(CO)_{12}]$	245	1.7	33	25	6	16	2	7	3	6	5.1	0.56
$Mn_2(CO)_{10}$	—	0.0	—	—	—	—	—	—	—	—	—	—
$K[HFe_3(CO)_{11}]$	233	1.7	43	16	6	17	2	7	2	7	4.1	0.59
$K[Fe_2Mn(CO)_{12}]$	251	1.6	35	27	2	18	—	10	—	7	22.5	0.61
HTR												
$Fe_3(CO)_{12}$–*A*	202	1.6	58	9	14	11	3	—	8	3	1.2	0.51
$Fe_3(CO)_{12}$–*B*	203	2.1	50	5	16	11	4	2	8	4	0.8	0.57
$NEt_4[Fe_2Mn(CO)_{12}]$	203	1.9	46	7	12	15	5	2	11	2	1.3	—
$Mn_2(CO)_{10}$	—	0.0	—	—	—	—	—	—	—	—	—	—
$K[HFe_3(CO)_{11}]$	232	2.0	45	13	6	20	2	5	4	5	4.1	0.53
$K[Fe_2Mn(CO)_{12}]$	227	1.3	32	17	1	22	1	18	1	9	24.5	—

7). As anticipated from older studies (*1, 2*), the presence of potassium in the KFe_3/C catalyst produced a large increase in the OPR, and gave a value of 4.1 after either treatment. The promotional effect of K was therefore not as dependent on the pretreatment as that of Mn. The $KMnFe_2/C$ catalyst yielded the highest OPRs and gave values of 23 after LTR and 25 after HTR. The effect of the addition of either K or Mn on the selectivity of Fe_3/C catalysts is similar, as either one increases the OPR; however, Mn favors light olefins and is more sensitive to the pretreatment. When both are added, the highest OPR values are obtained and they are nearly independent of pretreatment. The presence of K, though, markedly increases the rate of CO_2 formation relative to hydrocarbon (HC) production. Anderson–Schulz–Flory plots to obtain chain-growth probabilities are shown in Fig. 1 after LTR and in Fig. 2 after HTR. The α values calculated from Figs. 1a and 2a are listed in Table 4.

The activation energies for methanation, total HC formation, and CO_2 production are listed in Table 5. The somewhat lower values for the first two reactions over the K-free samples are consistent with previous studies of well-dispersed, C-supported Fe catalysts containing no K (*6, 13, 19, 20*). The addition of K to a cluster had a greater effect than Mn and it increased the activation energy, particularly after HTR. This behavior has been observed earlier (*6, 29*). The partial pressure dependencies following a HTR treatment are also given in Table 5, and the Fe-only catalysts exhibit a near first-order dependence on H_2 and a slightly negative dependence on CO. The addition of K to either cluster increased the total pressure dependence somewhat for both HC and CH_4 formation, but it still remained near first order. These results are again consistent with behavior reported for carbon-supported Fe catalysts (*6, 13, 19, 20*).

The results of the calorimetric investigation are summarized in Table 6. The integral CO heat of adsorption (Q_{ad}) following

TABLE 5

Kinetic Parameters of Fe–Mn/C Catalysts Derived from Metal Carbonyl Clusters

Catalyst	Activation energy (kJ/mole)			Partial pressure dependency[a]				
				HC[b]		CH_4		Temp.
	HC[b]	CH_4	CO_2	x	y	x	y	(K)
LTR								
$Fe_3(CO)_{12}$–*A*	73	71	111					
$Fe_3(CO)_{12}$–*B*	63	77	98					
$NEt_4[Fe_2Mn(CO)_{12}]$	53	67	86					
$Mn_2(CO)_{10}$	—	—	—					
$K[HFe_3(CO)_{11}]$	79	95	90					
$K[Fe_2Mn(CO)_{12}]$	69	83	81					
HTP								
$Fe_3(CO)_{12}$–*A*	84	82	95	0.8	−0.2	0.9	−0.1	240
$Fe_3(CO)_{12}$–*B*	73	74	92	0.8	−0.1	1.0	−0.2	253
$NEt_4[Fe_2Mn(CO)_{12}]$	70	72	92	0.4	0.4	0.9	0.0	262
$Mn_2(CO)_{10}$	—	—	—	—	—	—	—	—
$K[HFe_3(CO)_{11}]$	102	96	108	0.9	0.4	1.5	−0.3	262
$K[Fe_2Mn(CO)_{12}]$	106	94	94	1.0	0.3	1.3	−0.6	242

[a] $r = kP_{H_2}^x P_{CO}^y$.

[b] CO converted to hydrocarbons.

TABLE 6

Isothermal, Integral Heats of Adsorption of CO on Reduced Fe–Mn/C Catalysts at 300 K

Catalyst (sample run)	Chemisorption (μmoles CO/g cat)	Heat released (mcal/g cat)	Heat of adsorption (kcal/mole)	Q_{ad}[a] (kcal/mole)	$\frac{CO}{Fe_t}$
$Fe_3(CO)_{12}$–*A*				14.1 ± 0.7	
1–1	632	8573	13.6		0.41
1–2	458	6839	14.9		0.30
1–3	379	5254	13.9		0.24
2–1	—	8432	13.3[b]		—
2–2	—	6858	15.0[c]		—
$Fe_3(CO)_{12}$–*B*				15.9 ± 1.8	
1–1	389	6848	17.6		0.34
1–2	310	5457	17.6		0.27
1–3	350	4646	13.3		0.30
2–1	402	6614	16.5		0.35
2–2	368	5254	14.3		0.32
$NEt_4[Fe_2Mn(CO)_{12}]$				17.3 ± 1.0	
1–1	238	4063	17.1		0.27
1–2	219	3973	18.1		0.25
1–3	195	3644	18.7		0.22
2–1	240	4025	16.8		0.27
2–2	232	3694	15.9		0.26
$K[HFe_3(CO)_{11}$				16.6 ± 1.4	
1–1	140	2022	14.3		0.11
1–2	133	2126	16.0		0.10
1–3	128	2130	16.6		0.10
2–1	121	2120	17.5		0.10
2–2	112	2083	18.6		0.09
$K[Fe_2Mn(CO)_{12}]$				20.7 ± 1.2	
1–1	186	3609	19.4		0.20
1–2	174	3408	19.6		0.18
1–3	163	3357	20.6		0.17
2–1	172	3871	22.5		0.18
2–2	170	3643	21.4		0.18

[a] Average values with standard deviations.
[b] Chemisorption of 632 μmoles CO/g cat assumed.
[c] Chemisorption of 458 μmoles CO/g assumed.

HTR for each catalyst was determined for two samples, and the measurements were repeated at least once on each sample. The results for Fe_3/C–*A* yielded a Q_{ad} value of 14.1 ± 0.7 kcal/mole, while those for Fe_3/C–*B* gave a value of 15.9 ± 1.8 kcal/mole. The average of these two catalysts is 15.0 kcal/mole; however, the standard deviations imply this may be on the high side. The addition of Mn to the cluster gave a higher value of 17.3 ± 1.0 kcal/mole for Fe_2Mn/C, and the addition of K also increased the Q_{ad} value, which was 16.6 ± 1.4 kcal/mole for KFe_3/C. The coaddition of these two elements to give the KFe_2Mn/C catalyst yielded the highest Q_{ad} value of 20.7 ± 1.2 kcal/mole. These results indicate that the effect of each promoter is additive, and the strongest CO adsorption occurs on the doubly promoted catalyst.

The effect of successive reduction/CO chemisorption cycles on the different catalysts is also clearly demonstrated in Table 6. It is more striking for the Fe_3/C–*A* catalyst, for which the CO adsorption decreased by 42% after 3 cycles, but the total

heat released decreased by a similar amount to yield relatively constant Q_{ad} values. The Fe_3/C catalysts seemed susceptible to sintering during these HTR/adsorption cycles. Mn addition, as illustrated by the Fe_2Mn/C catalyst, gave a lower initial dispersion but increased stability as CO uptakes decreased only 18% after 3 HTR cycles. The addition of K, however, decreased dispersion and enhanced sintering as indicated by the KFe_3/C and KFe_2Mn/C catalysts, with the former having the lowest dispersion. The role of potassium in enhancing the sintering of Fe has been recognized before (*30*).

DISCUSSION

Well-dispersed, carbon-supported Fe–Mn catalysts have been found to be very active for CO hydrogenation while at the same time retaining a very high selectivity for light olefins (*6, 7*). These initial kinetic results prompted an extensive effort to characterize these Fe/C, Fe–Mn/C, and K–Fe–Mn/C catalysts by a variety of techniques including MES (Mössbauer effect spectroscopy), TEM/EDS, DRIFTS, adsorption, calorimetry, and kinetic behavior (*8, 9*). The focus of these studies was to elucidate the nature of the Fe–Mn interaction during and after decomposition of the carbonyl cluster precursors and to obtain a better understanding of the chemical state of these catalysts. To facilitate characterization by MES and detection by DRIFTS, the catalysts prepared here had higher metal loading than those in our previous study, but despite this they maintained similar catalytic and adsorption behavior, and the catalysts without K in the cluster were also well dispersed.

The discussion of the catalysts investigated here will be broken into two sections—the first pertains to the LTR family and the second describes the series after HTR. Within each section, the chemistry associated with the genesis of the Fe_2Mn/C and KFe_2MN/C samples will be emphasized, final states of the catalysts will be proposed, and the adsorption and catalytic behavior will then be related to these models.

LTR (Low Temperature Reduction) Catalysts

The two previous studies in this series reported DRIFTS (*8*) and MES (*9*) results showing that $Fe_3(CO)_{12}$ clusters on this carbon partially decompose to $Fe(CO)_5$ and zero-valent iron at 30 K, and heating to 473 K completely decarbonylates both species, with no detectable intermediate species formed, to give highly dispersed iron. These Fe particles are described by a "*D*-structure," proposed to consist of superparamagnetic Fe along with an Fe^{2+} state formed by oxygen atoms which also interact with the carbon surface (*21*). As we have previously discussed, we consider the central superparamagnetic singlet and the Fe^{2+} doublet which has routinely been observed for carbon-supported iron to be characteristic of a specific structure associated with the carbon surface (*21*). The arguments for this assignment have been given in the second paper in this series (*9*), and they consist primarily of the observation that the Fe^0 and Fe^{2+} peak intensities vary in concert and thus their relative peak area ratios remain essentially constant and, in addition, that this behavior has been observed only when amorphous, high surface area carbon is utilized. The DRIFTS study showed that $Mn_2(CO)_{10}$ clusters also decomposed straightforwardly, with the final product assumed to be Mn oxide (*8*). The importance of an oxygen-free surface is revealed, even at this point, by the decomposition process of $Fe_3(CO)_{12}$. On oxide surfaces containing hydroxyl groups, the transformation of $Fe_3(CO)_{12}$ to $[HFe_3(CO)_{11}]^-$, via $Fe(CO)_5$ as an intermediate, is well known (*12* and references therein). It is also known that the reaction of $Fe(CO)_5$ to give $[HFe_3(CO)_{11}]^-$ in solution or on oxide surfaces requires hydroxyl groups (*31*). Consequently, the absence of

any hydroxyl groups on this carbon precluded the formation of this species.

Although the Fe_2Mn carbonyl clusters examined in this study demonstrated a simple decomposition process under He, they exhibited more complicated behavior under H_2 as both $NEt_4[Fe_2Mn(CO)_{12}]$ and $K[Fe_2Mn(CO)_{12}]$ decomposed initially to give $Mn_2(CO)_{10}$ and an Fe hydrido-carbonyl cluster (*8*). The DRIFTS study identified the Mn cluster as an intermediate, and only the $[HFe_4(CO)_{13}]^-$ anion gives both IR and MES spectra in agreement with those obtained (*8, 9*); thus, the combined use of these two techniques allowed us to eliminate all other Fe carbonyl clusters. These two intermediates then continued to decompose during the LTR step at 473 K to form the final, highly dispersed catalyst, with MES indicating that the Fe is present as the *D*-structure (*9, 21*).

Although the direct combination of two $[Fe_2Mn(CO)_{12}]^-$ anions provides the appropriate stoichiometry to give the observed $Mn_2(CO)_{10}$ and $[HFe_4(CO)_{13}]^-$ intermediates species, this is an improbable reaction, and solution chemistry studies suggest an alternate pathway. Based on the work of Seder *et al.* (*32*), it is proposed that $[Fe_2Mn(CO)_{12}]^-$ clusters fragment during the decarbonylation process under H_2 to yield mononuclear Mn species (possibly $Mn(CO)_5$ radicals) which quickly recombine to form $Mn_2(CO)_{10}$. The decomposition of the initial cluster also yields iron pentacarbonyl, other iron-containing carbonyl clusters, and zero-valent iron in the *D*-structure. The Fe^0 atoms can dissociate H_2, and the presence of these H atoms can markedly influence the cluster chemistry. Although speculative at this time, it is possible that anionic iron carbonyl species are bound to the positive-valent Fe atoms contained within the *D*-structure, and thus would have access to the hydrogen atoms adsorbed on neighboring Fe^0 atoms. It is further proposed that during cluster fragmentation small amounts of $[Fe(CO)_4]^{-2}$ species form (*33–36*). This is a highly reactive species and in the presence of dissociated hydrogen could readily form a $[HFe(CO)_4]^-$ species which acts as a building block for the higher nuclearity Fe carbonyl anions. This chemistry is similar to reactions involving $[Fe(CO)_4]^{-2}$ species that occur in solution (*33–36*). Thus, $[HFe(CO)_4]^-$ reacts rapidly with $Fe(CO)_5$ to form $[HFe_2(CO)_8]^-$, which in turn reacts with $Fe(CO)_5$ to form $[HFe_3(CO)_{11}]^-$, which then finally reacts with $Fe(CO)_5$ to form the most stable tetranuclear $[HFe_4(CO)_{13}]^-$ cluster. This reaction sequence relies on steps reported for Fe clusters in solution in the absence of oxygen (*33–36*). The fact that no $[HFe(CO)_4]^-$, $[HFe_2(CO)_8]^-$, and $[HFe_3(C)_{11}]^-$ species were detected by either DRIFTS or MES indicates their higher reactivity and is consistent with the fact that four iron atoms represent the highest nuclearity in iron carbonyl clusters because of the stability of tetrahedral bonding.

The necessity of incorporating atomic hydrogen into the Fe cluster to form the initial intermediate, $[HFe(CO)_4]^-$, is indicated by the straightforward decomposition of the $[Fe_2Mn(CO)_{12}]^-$ anion under He (*8*). Although the original cluster fragments into separate Fe- and Mn-containing clusters, the metals remain in intimate contact, as explained later. The $Mn_2(CO)_{10}$ cluster finally decomposes into a MnO_x species, where x is assumed to be near unity. This conclusion is supported by the recent study of $Co–Mn/SiO_2$ catalysts by Klabunde and co-workers, who used EXAFS to show that MnO was formed in this system (*37*).

The decomposition model suggested for carbon-supported clusters containing the $[Fe_2Mn(CO)_{12}]^-$ anion during LTR is summarized in Table 7. The reactions are not balanced because it is possible for dissociative CO adsorption to occur on the Fe particles formed during decomposition (*38, 39*), hence the exact amount of gas-phase CO produced is not known. All the Fe-containing catalysts, with or without K promotion, yielded small crystallites of Fe present in the *D*-structure, whose possible origin and

TABLE 7

Decomposition Pathway for Clusters Containing the $[Fe_2Mn(CO)_{12}]^-$ Anion

(I) $[Fe_2Mn(CO)_{12}]^- \rightarrow Fe(CO)_5 + Fe(D\text{-structure}) + Mn_2(CO)_{10} + CO$
(II) $[Fe_2Mn(CO)_{12}]^- + H_2 + D\text{-structure} \rightarrow Fe(CO)_5 + [HFe(CO)_4]^- + Mn_2(CO)_{10}$
(III) $Fe(CO)_5 + [HFe(CO)_4]^- \rightarrow [HFe_2(CO)_8]^- + CO$ (rapid)
(IV) $Fe(CO)_5 + [HFe_2(CO)_8]^- \rightarrow HFe_3(CO)_{11}]^- + CO$ (rapid)
(V) $Fe(CO)_5 + [HFe_3(CO)_{11}]^- \rightarrow [HFe_4(CO)_{13}]^- + Fe[D\text{-structure}]$ (rapid)
(VI) $Mn_2(CO)_{10} \rightarrow MnO_x\ (x \approx 1) + CO + C$

nature are discussed in detail elsewhere (*9, 21*). MES did not detect the presence of either α-Fe or the mixed Fe_2MnO_4 spinel, but small quantities of Fe^{3+} were detected and are assumed to be present on the surface of these particles. Because of its high oxygen affinity, the Mn is presumed to be present as an oxide, MnO_x, with x expected to be close to 1 (*37*). The oxygen is provided by dissociated CO ligands. The MnO_x phase is presumed to be present on the surface of these Fe particles, possibly as two-dimensional rafts, and we have reported evidence for a mixed Fe–Mn oxide phase (*9*). The low CO chemisorption uptakes after LTR also imply that a large fraction of the iron surface is covered. One conceptual representation of the final state of these Fe_2Mn/C catalysts is depicted in Fig. 3a.

Although a surface Fe_2Mn spinel structure cannot be completely ruled out because of the decrease in sensitivity of MES related to Fe surface phases (*40*), the absence of any MES peaks associated with this species argues against its presence, at least in significant quantities. Thus the explanation proposed by two of us (*6*) relating the high selectivity to light olefins to the Fe_2MnO_4 spinel structure is not supported by these results. However, the patches of MnO_x which cover the Fe particles can provide a large interfacial area, and special sites may exist in this region to activate CO, either by a localized promoter effect or by direct interaction with the oxygen end of the CO molecule (*41*). This coupled with a decrease in the surface coverage of hydrogen could produce the observed behavior. We prefer the latter model as none of the large quantities of adsorbed CO was detected by IR, consistent with the presence of tilted CO species with very low wave numbers or CO strongly bonded through both the C and the O atoms, or dissociated CO (*38, 39*). The additional presence of K would further facilitate CO dissociation. An additional important aspect of the relationship of catalytic behavior to these well-dispersed, promoted, carbon-supported Fe particles is the surface coverage of hydrogen. Hydrogen adsorption on small Fe crystallites is decreased relative to CO adsorption (*13, 28*) and, because of the first-order dependence on H_2, this may be the primary reason that TOFs are lower and the olefin/paraffin ratios (OPR) are somewhat higher on these Fe surfaces. The results in Table 3 imply that hydrogen coverages remain low on the LTR catalysts thereby giving high OPRs.

The exact chemical state of the metal particle surface is still not known, but the catalytic properties, such as TOF, OPR, and activation energies (Table 5), of each member of the LTR family are similar to those of its HTR counterpart. Thus, these kinetic parameters imply that the surface state of the LTR catalysts under reaction conditions is similar to that of the HTR catalysts. One noticeable difference is the lower activation energy for the LTR K-promoted catalysts. Reasonable fits of the Anderson–Schulz–Flory distribution are obtained up to C_6 when both olefins and paraffins are included, as shown in Fig. 1a, with the KFe_3/C catalyst exhibiting the

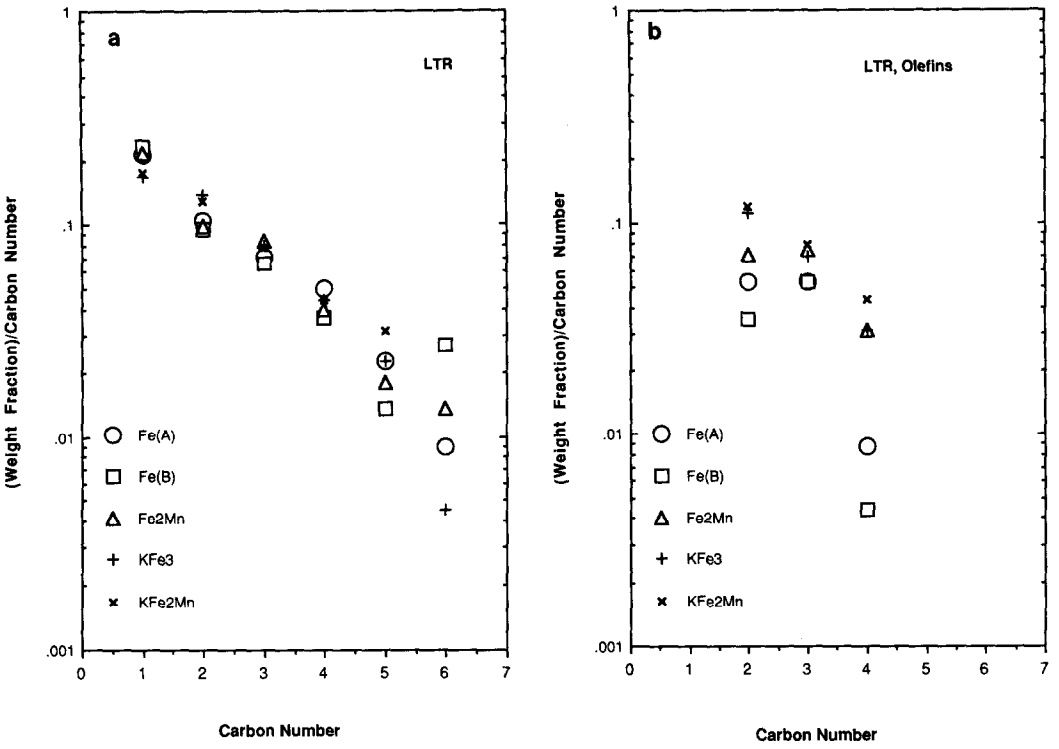

FIG. 1. Anderson–Schulz–Flory (ASF) plots for carbon-supported, cluster-derived catalysts after LTR at 473 K; P = 0.1 MPa, H_2/CO = 3, T = 474–518 K (see Table 4): (a) total hydrocarbons (olefins + paraffins); (b) olefins only.

greatest deviation. A similar plot for C_2–C_4 olefins (Fig. 1b) gives a good fit only for the KFe_2Mn/C catalyst. The C_5–C_6 olefins could not be easily resolved from the C_5–C_6 paraffins. The presence of potassium does not appear to have a large effect on the α value. Finally, the extremely high light olefin yields obtained with the LTR KFe_2Mn/C catalyst should be noted. They are consistent with our previous results although the higher iron loading appears to decrease the OPR somewhat and to increase chain-growth probability.

HTR (High Temperature Reduction) Catalysts

A HTR treatment can significantly alter the metal morphology when potassium is present as well as influence the kinetic and adsorption behavior of these catalysts. MES spectra showed that the Fe_3/C catalysts contained well-dispersed particles consisting of approximately 80% *D*-structure and 20% α-Fe, while the Fe_2Mn/C catalyst retained the highly dispersed, *D*-structure particles present after LTR (*9*). The inability to observe metal particles by TEM (*9*) and the CO adsorption values listed in Table 1 also indicated that the particles in the latter sample did not increase significantly in size during HTR. After CO adsorption at 300 K the reformation of significant amounts of $Fe(CO)_5$ in the Fe_3/C catalyst, and to a lesser degree for Fe_2Mn/C, was observed, but virtually no such species was formed on the K-promoted catalysts. This capability to form iron pentacarbonyl has been found only with highly dispersed iron (*8*, *9*, *21*). No surface CO species other than $Fe(CO)_5$ was detected by DRIFTS for any of the catalysts, showing that adsorbed CO was again

present in an IR-inactive form. The proposed state of the catalyst is depicted in Fig. 3b.

By comparison, as determined by MES and TEM results (*9*) the catalysts containing K appeared to sinter significantly and produce large (ca. 30 nm) α-Fe particles, with the micrographs showing that the metal particles on this high surface area carbon were indistinguishable from those formed on graphite (*42*). This behavior is consistent with our earlier work and supports the proposal that active sites on the carbon surface can facilitate the nucleation and stabilization of small iron particles. When the surface was not cleaned by a treatment at 1125 K, sintering occurred in these Fe/C catalysts, but this cleaning treatment combined with an anaerobic catalyst preparation method resulted in a highly dispersed Fe catalyst (*21*). The catalyst in the sintered state is illustrated in Fig. 3c.

In this study of promoted Fe catalysts, it was found that the active sites on carbon again appear to play a significant role in determining the stability and final morphology of the metallic structures. The presence or absence of available active sites can explain the differences in morphology between samples with and without potassium; i.e., for samples without potassium the carbon active sites can act as nucleation sites and stabilize small metal particles, whereas when potassium is present it poisons these active sites and prevents the interaction which produces this stabilization. This suggestion is consistent with previous observations that potassium will "spread" on high surface area carbon samples at high temperatures (*43*). It is also consistent with calorimetric results which show that potassium, added as a carbonate by physical mixing and then heated to high temperature, blocks carbon active sites on coal chars (*44*). As shown in a prior study, a high surface area carbon without active sites will behave very much like graphite (*21*). Indeed, the structural development of the metal particles produced from the clusters containing potassium is almost identical to that found when particles were made by the thermal decomposition of Fe–Mn clusters containing no potassium on a graphitic support; that is, the particles sinter rapidly, there is phase separation between the iron and manganese after high temperature reduction, and large hollow spheres form during oxidation (*42*). All this suggests that there is direct interaction between the metal in the clusters and the active sites on the carbon surface when there is no potassium present to preferentially block the sites.

Although the decreased CO uptakes at 300 K on either the fresh or the used HTR potassium-containing catalysts are consistent with the formation of large iron particles, as depicted in Fig. 3c, the high CO uptakes at 195 K are not. This may be a consequence of the influence of potassium at this temperature on promoted Fe surfaces; however, if the adsorption at 195 K is unaffected, as indicated by the work of Emmett and Brunauer (*15*), it could also mean that these larger particles are agglomerates of smaller Fe crystallites mixed with MnO phases. As mentioned previously, because of interaction anisotropy the Mössbauer spectrum would still appear to be that of α-Fe (*45*); thus, there is a possibility that the system may be that indicated in Fig. 3d. The similarity in TOF values among the different catalysts is also supportive of this picture.

Consequently, our perception of the state of the Fe/C and Fe_2Mn/C catalysts after HTR is that the iron still exists as small particles, primarily in the *D*-structure, although some particle growth may have occurred. If Mn is present, it now exists as three-dimensional MnO_x crystallites under reaction conditions with a reduced interfacial contact with the iron surface, as shown in Fig. 3b. The decreased effect on the OPR supports this picture. MES provides evidence that a mixed Fe–Mn oxide phase may exist immediately after the HTR step. As mentioned, the addition of K can induce

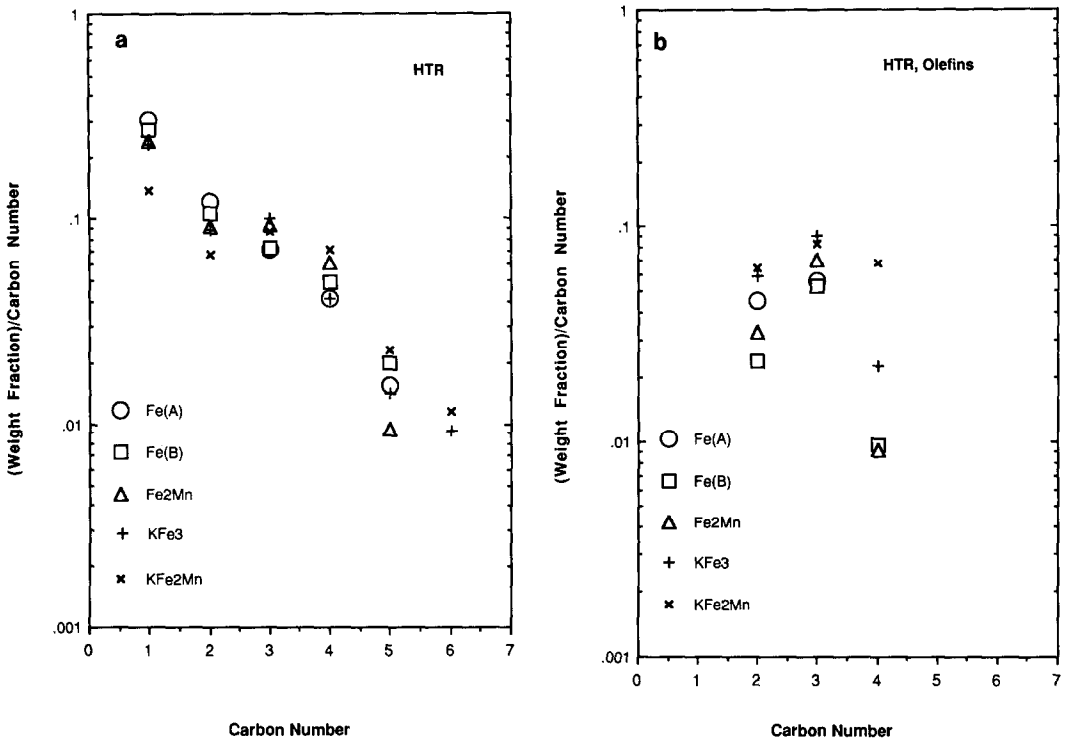

FIG. 2. Anderson–Schulz–Flory (ASF) plots for carbon-supported, cluster-derived catalysts after HTR at 673 K; P = 0.1 MPa, H_2/CO = 3, T = 475–505 K (see Table 4): (a) total hydrocarbons (olefins + paraffins); (b) olefins only.

sintering and the formation of large (20–40 nm) α-Fe particles or α-Fe phases mixed with MnO phases. When fitted to an Anderson–Schulz–Flory distribution (Fig. 2a), these HTR catalysts exhibit a somewhat lower α value and more deviation, with higher than expected C_3–C_4 contents. The high fractions of light olefins do not fit this distribution, as shown in Fig. 2b, similar to the behavior of the LTR family of catalysts. The high yields of light olefins reported earlier for HTR KFe_2Mn/C are again reproduced on these catalysts with higher Fe loading; however, as noted for the LTR sample, the selectivity to C_2–C_4 olefins is somewhat lower because the OPR is slightly lower and the chain-growth probability to C_{5+} hydrocarbons is higher. The reasonable fits to the Anderson–Schulz–Flory distribution when both olefins and paraffins are included, especially for the LTR catalysts, produces an interesting implication—the total chain-growth rate divided by the overall termination rate (α) remains constant, but the olefin behavior alone does not conform. One interpretation is that chain-growth is similar for both olefins and paraffins and rates of olefin desorption are comparable to rates of hydrogenation. The presence of the potassium may stabilize the contact between the iron surface and the Mn oxide, though, because the TOF and OPR values of the LTR and HTR KFe_2Mn/C catalysts are similar. As shown in Table 4, after either a LTR or HTR treatment, the KFe_2Mn/C catalyst produces very high OPRs near 24 and exceptionally high yields or light olefins. This confirms previous studies in which lower metal loadings were used and even higher yields were obtained (*6, 7*). In addition, as discussed next, the highest Q_{ad} values for CO were

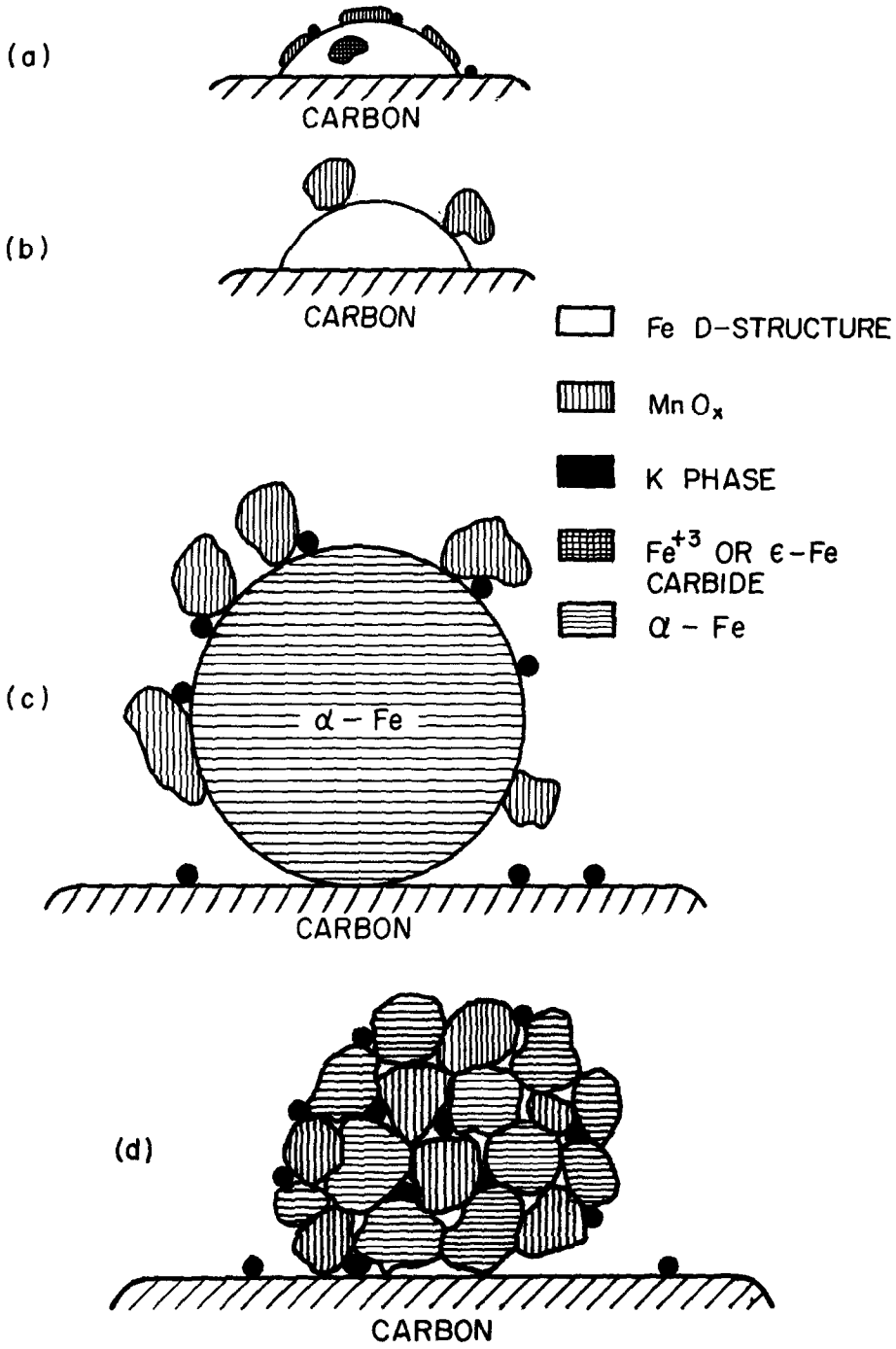

FIG. 3. (a) Proposed state of K–Fe–Mn/C catalysts after LTR; Fe–Mn/C catalysts are presumed to be similar, only the K phase is absent. The iron particles are small (<4 nm) and exist primarily in the *D*-structure (see text). (b) Proposed state of Fe–Mn/C catalysts after HTR. The Fe particles remain small and still exist in the *D*-structure, and the Mn oxide has sintered into three-dimensional particles. (c) One possible state of K–Fe–Mn/C catalysts after HTR. The iron has sintered, along with the Mn oxide, to form large ferromagnetic α-iron (>30 nm) crystallites. (d) Alternate state of K–Fe–Mn/C catalysts after HTR. Small zero-valent iron phases are mixed with MnO phases to form a larger composite particle. Because of their proximity and the interaction anisotropy these Fe particles give a Mössbauer spectrum comparable to that of ferromagnetic α-Fe crystallites.

obtained for the HTR KFe_2Mn/C sample, and they seemed to indicate an additive effect from each promoter, which would imply the presence of both on the iron surface.

The calorimetric measurements showed that the addition of either Mn or K has a detectable effect on the CO heats of adsorption on Fe after HTR, as the Q_{ad} value of 15.0 kcal/mole for the Fe_3/C catalyst increased to 17.3 kcal/mole for the Fe_2Mn/C catalyst and to 16.6 kcal/mole for the KFe_3/C catalyst. Addition of both promoters gave a value of 20.7 kcal/mole for the KFe_2Mn/C catalyst. The effect of the K and Mn on the Q_{ad} values appears to be additive and, at the very least, indicates that both Mn and K cause an increase in the Q_{ad} values, thereby implying that they are in contact with the Fe phase. This information was assimilated into our conception of the catalyst after HTR, shown in Fig. 3c.

The kinetic parameters in Table 5 do not reveal any marked differences among the activation energies for HC or CH_4, with the exception of higher E_{act} values for HC formation on the HTR K-promoted samples. This has been observed previously (*6*). Also consistent with previous results are the near first-order overall dependences on pressure, i.e., the sum of $x + y$ in Table 5. Of particular importance is the similarity in the OPR after LTR and after HTR for both the KFe_3/C and KFe_2Mn/C catalysts. We conclude from this that the surface states are similar after either pretreatment even though the Fe particle sizes may be much larger after HTR.

In summary, a reaction sequence for Fe_2Mn and KFe_2Mn cluster decomposition on carbon is proposed which involves monometallic cluster intermediates and is based upon previous MES, DRIFTS, and solution chemistry studies. In the absence of K, either a LTR or a HTR pretreatment produces well-dispersed Fe catalysts; however, addition of K to the cluster results in substantial particle growth during HTR. Despite this, the surfaces of the K-promoted and doubly promoted (K + Mn) LTR and HTR samples under reaction conditions produce similar catalytic behavior in most aspects, at least under low conversions where reducing conditions are maintained, as OPR and TOFs were comparable and α values were nearly the same although the promoted HTR catalysts exhibited greater deviations from the Anderson–Schulz–Flory distribution. The CO heats of adsorption on these catalysts after HTR indicated that the addition of either Mn or K increased Q_{ad} values, and this effect was additive as the doubly promoted sample gave the highest value, with an increase in Q_{ad} close to the sum of the increments produced by the two promoters separately. This implies that both the Mn and K species are in contact with the Fe surface atoms, and it is likely that the phases containing K and Mn are in direct contact with each other as well as the iron surface.

ACKNOWLEDGMENTS

This study was supported by the National Science Foundation under Grant CBT-8619619. Partial support of A. A. Chen by a Texaco Philanthropic Foundation Fellowship is gratefully noted. Discussions with Professor G. L. Geoffroy regarding cluster fragmentation chemistry are greatly appreciated.

REFERENCES

1. Storch, H. H., Golumbic, N., Anderson, R. B., "The Fischer–Tropsch and Related Syntheses." Wiley, New York, 1951.
2. Emmett, P. H., "Catalysis," Vol. 4. Reinhold, New York, 1956.
3. Kolbel, H., and Tillmetz, K. D., Belgian Patent 837628.
4. Kolbel, H., and Ralek, M., *Catal. Rev. Sci. Eng.* **21,** 227 (1980).
5. Kolbel, H., Ralek, M., and Tillmetz, K. D., "13th Int. Soc. Eng. Conv. Soc. Aut. Eng., 482 (1982).
6. Venter, J. J., Kaminsky, M., Geoffroy, G. L., and Vannice, M. A., *J. Catal.* **103,** 450 (1987).
7. Venter, J. J., Kaminsky, M., Geoffroy, G. L., and Vannice, M. A., *J. Catal.* **105,** 155 (1987).
8. Venter, J. J., Chen, A. A., and Vannice, M. A., *J. Catal.* **117,** 170 (1989).
9. Chen, A. A., Phillips, J., Venter, J., and Vannice, M. A., *J. Catal.*, in press.
10. Phillips, J., and Dumesic, J. A., *Appl. Catal.* **9,** 1 (1984).

11. Venter, J., Kaminsky, M., Geoffroy, G. L., and Vannice, M. A., *in* "Preparation of Catalysts, IV" (B. Delmon *et al.*, Eds.). p. 479. Elsevier, Amsterdam, 1987.

12. Venter, J. J., and Vannice, M. A., *J. Phys. Chem.* **93,** 4158 (1989).

13. Jung, H. J., Walker, P. L., and Vannice, M. A., *J. Catal.* **75,** 416 (1982).

14. Vannice, M. A., Walker, P. L., and Jung, H. J., Moreno-Castilla, C., and Mahajan, O. P., "Proc. 7th Int. Cong. Catal., p. 460. Elsevier, Amsterdam, 1981.

15. Emmett, P. H., and Brunauer, S., *J. Amer. Chem. Soc.* **59,** 310 (1937).

16. Amelse, J. A., Schwartz, L. H., and Butt, J. B., *J. Catal.* **72,** 95 (1981).

17. Vannice, M. A., *J. Catal.* **37,** 449 (1975).

18. Sen, B., Chou, P., and Vannice, M. A., *J. Catal.* **101,** 517 (1986).

19. Jung, H. J., Vannice, M. A., Mulay, L. N., Stanfield, R. M., and Delgass, W. N., *J. Catal.* **76,** 208 (1982).

20. Kaminsky, M., Yoon, K. J., Geoffroy, G. L., and Vannice, M. A., *J. Catal.* **91,** 338 (1985).

21. Chen, A. A., Vannice, M. A., and J. Phillips, *J. Phys. Chem.* **91,** 6257 (1987).

22. Jensen, K. B., and Massoth, F. E., *J. Catal.* **92,** 109 (1985).

23. Lohrengel, G., and Baerns, M., *Ber. Bunsenges. Phys. Chem.* **87,** 335 (1983).

24. Barrault, J., Forquy, C., and Perrichon, V., *Appl. Catal.* **5,** 119 (1983).

25. Barrault, J., and Renard, C., *Appl. Catal.* **14,** 133 (1985).

26. Ford, R. F., *Adv. Catal.* **21,** 51 (1970).

27. Bickley, R. I., Roberts, M. W., and Storey, W. C., *J. Chem. Soc. A,* 2774 (1971).

28. Topsoe, H., Topsoe, N., and Bohlbro, H., "Proceedings 7th Intl. Cong. Catal., Tokyo (1980)," p. 247. Elsevier, Amsterdam, 1981.

29. McVicker, G. B., and Vannice, M. A., *J. Catal.* **63,** 25 (1980).

30. Dry, M. E., and Ferreira, L. C., *J. Catal.* **7,** 352 (1967).

31. Hansen, B. E., Bergmaester, J. J., Petty, J. T., and Connaway, M. C., *Inorg. Chem.* **25,** 3089 (1986).

32. Seder, T. A., Church, P., and Weitz, E., *J. Amer. Chem. Soc.* **108,** 1084 (1986).

33. Hieber, V. W., and Beutner, H., *Z. Naturforsch. B: Anorg. Chem. Org. Chem.* **17,** 211 (1962).

34. Hieber, V. W., and Brendel, G., *Z. Anorg. Chem.* **289,** 324 (1957).

35. Hieber, V. W., and Brendel, G., *Z. Anorg. Chem.* **289,** 338 (1957).

36. Kaesz, H. D., and Saillant, R. B., *Chem. Rev.* **72,** 231 (1972).

37. Tan, B. J., Klabunde, K. J., Tanaka, T., Kanai, H., and Yoshida, S., *J. Amer. Chem. Soc.* **110,** 5951 (1988).

38. Cameron, S. D., and Dwyer, D. J., *Langmuir* **4,** 282 (1988).

39. Moon, D. W., Cameron, S. D., Zaera, F., Eberhardt, W. Carr, R., Bernasek, S. L., Gland, J. L., and Dwyer, D. J., *Surf. Sci. Lett.* **180,** L123 (1987).

40. Gatte, R., and Phillips, J., *Langmuir* **5,** 756 (1989).

41. Vannice, M. A., and Sudhakar, C., *J. Phys. Chem.* **88,** 2429 (1984).

42. Chen, A. A., Vannice, M. A., and Phillips, J., *J. Catal.* **116,** 568 (1989).

43. Mims, C. A., Chludzinski, J. J., Pabst, J. K., and Baker, R. T. K., *J. Catal.* **89,** 97 (1984).

44. Gow, A., and Phillips, J., unpublished results.

45. Morup, S., Dumesic, J. A., and Topsoe, H., *in* "Applications of Mössbauer Spectroscopy" (R. L. Cohen, Ed.), Vol. II, p. 1. Academic Press, New York, 1980.